

PCCP

Accepted Manuscript



This is an *Accepted Manuscript*, which has been through the Royal Society of Chemistry peer review process and has been accepted for publication.

Accepted Manuscripts are published online shortly after acceptance, before technical editing, formatting and proof reading. Using this free service, authors can make their results available to the community, in citable form, before we publish the edited article. We will replace this *Accepted Manuscript* with the edited and formatted *Advance Article* as soon as it is available.

You can find more information about *Accepted Manuscripts* in the [Information for Authors](#).

Please note that technical editing may introduce minor changes to the text and/or graphics, which may alter content. The journal's standard [Terms & Conditions](#) and the [Ethical guidelines](#) still apply. In no event shall the Royal Society of Chemistry be held responsible for any errors or omissions in this *Accepted Manuscript* or any consequences arising from the use of any information it contains.

ARTICLE

Self-healing Dynamic Bond-based Rubbers: Understanding the Mechanisms in Ionomeric Elastomer Model Systems

Cite this: DOI: 10.1039/x0xx00000x

N. Hohlbein¹, A. Shaaban¹, A. R. Bras², W. Pyckhout-Hintzen², A. M. Schmidt^{1*}Received 00th January 2012,
Accepted 00th January 2012

DOI: 10.1039/x0xx00000x

www.rsc.org/

While it is traditionally accepted that the chain interactions responsible for the elastic response in an elastomeric network are ideally permanent and instantaneously active, the ongoing investigation of self-healing materials reveals that the introduction of self-healing properties to elastomers requires both: high mechanical integrity under dynamic load conditions, while on long timescales (or at extended temperatures), the chain and bond dynamics allow for an intrinsic repair of micro cracks occurred during operation and aging. Based on an acrylate-based amorphous ionomer model system with pending carboxylate groups allowing the systematic variation of the composition and the nature of the counter ion, we demonstrate the interrelation of the morphological, thermal, and mechanical properties, and identify the prerequisites and tools for property adjustment and optimization of the self-healing efficiency. While the ion fraction is directly related to the effective network density and elastic performance, the crossover frequency between viscous and elastic behavior is influenced by the nature of the counter ion. In order to result in reliable elastic response and optimal damage repair, the ion fraction in these systems is in the range of 5 mol%, while the chain dynamics is still sufficient to allow for excellent self-healing behavior observed at moderate healing temperatures.

Introduction

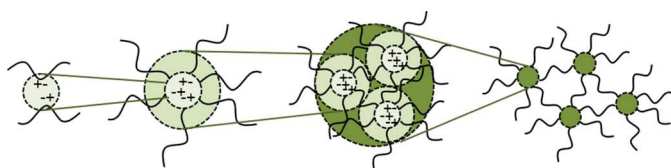
The design of innovative supramolecular polymers with novel or improved characteristics is an important segment in today's research on synthetic materials. The ease of chemical modification, a broad variety of functionalities in combination with interesting physical properties and structure-property relationships distinguish these compounds for the development of materials with new functions, such as multi-stimuli responsiveness, self-cleaning, self-assembly or self-healing, and has already resulted in the development of exceptional adaptive and smart materials.¹⁻⁶

In particular, supramolecular polymers tailored with respect to their self-healing ability entered the focus of interest during the past decade. The intrinsic ability of self-healing is one of the most remarkable bio-inspired concept for synthetic materials.⁷ Non-autonomic approaches require an external trigger but in advantage, the healing process can be activated performed in a controlled way.⁸ Dynamic-bond based systems founded on e. g. hydrogen bonds, metal-ligand coordination or ionic interaction, offer the possibility of multiple healing and can be made responsive to a wide range of stimuli.⁹⁻¹²

In particular, self-healing polymers based on the presence of ionic aggregates in unpolar matrices, known as ionomers,¹³⁻¹⁷ have recently been demonstrated to be a powerful approach towards commercially interesting self-healing thermoplasts,

elastomers, and coatings.¹⁸⁻²⁶ However, a profound understanding of the underlying structure-property correlations is required to allow a tailored optimization of these materials for a given application.

Ionomers are usually constituted by an unpolar main chain with random, blocked or grafted ionic units with an ion fraction below 15 mol%. The characteristic feature is the organization into a dynamic and thermoreversible supramolecular network based on the phase separation into an ion-rich and an ion-poor subphase. Based on the Eisenberg-Hird-Moore (EHM) model, the ion-rich phase is constituted of ionic multiplets, consisting of a limited number of chain-attached ions and their respective counter-ions embedded into a polymeric area of restricted mobility (Scheme 1).^{13,14} At higher ion fractions, the multiplets are further organized into bigger clusters that may be of fractal or string-like shape, depending on the properties of both the ionic groups and the bulk polymer segments. While ionomers are well studied since the 1980s and are commonly used in commercial applications like packaging, sports equipment etc.,¹⁵⁻¹⁷ a first report on their interesting intrinsic self-healing properties appeared in 2007 on semicrystalline systems based on ethylene-methacrylic acid copolymers.^{19,26} Up to date, a dominating number of studies concerning self-healing ionomers are based on similar semicrystalline systems, and the presence of a crystalline component plays an important role in the healing process, as was clearly demonstrated.¹⁹



Scheme 1. EHM model for the hierarchical structure formation in ionomers: ion pair – multiplet – ionic cluster – network, with encircled regions of restricted polymer mobility.

With the detection of self-healing properties also in non-vulcanized, ionomeric groups containing NBR-based rubber materials, the approach became of particular interest for the development and optimization of self-healing ionomeric elastomers.²⁷

The comparably long lifetime of the ionic association gives rise to a good mechanical performance under dynamic load typical for a thermoplastic elastomer, while on the other hand still allows for sufficient molecular mobility to result in self-healing behavior upon damage. Important for commercialization is that the intrinsic nature of the effect based on polymer-attached ions is in accordance with the drastic processing conditions in ionomers. In addition, ionic elastomers are able of storing the elastic energy on multiple time scales, and their variable network density of reversible aggregates features them for self-healing applications.

It is thus the objective of the present study to systematically investigate the influence of the ionic fraction and the nature of the counter-ion on the mechanical and self-healing properties of amorphous ionomers with a flexible main chain, and to correlate the findings to their structural and thermal characteristics. This systematic study thus targets at the self-healing efficiency of a model system that is dominantly crosslinked by the ion aggregates, and allows the systematic variation of the composition and the direct investigation of its impact on the materials performance based on a broad range of methods.

A suitable approach is based on atom-transfer radical copolymerization (ATRP) of *n*-butyl acrylate (*n*BA) and *tert*-butyl acrylate (*t*BA) with subsequent hydrolysis of the *tert*-butyl ester groups followed by neutralization with different cations.²⁸ Due to the similar reactivity of the comonomers,^{29,30} random copolymers with a predetermined molar mass, narrow polydispersity,³¹ and adjustable composition are obtained. The materials are characterized with respect to their molecular and bulk structure by ¹H-NMR, ATR-IR, DSC and SAXS, respectively, and their dynamic and quasi-static mechanical properties and self-healing potential are systematically investigated. The results are of general importance for the understanding, and contribute to the optimization, of the healing mechanism in similar, dynamic bond-based self-healing elastomers.

Experimental section

Materials

n-Butyl acrylate (*n*BA, Aldrich, 99%) and *tert*-butyl acrylate (*t*BA, Aldrich 98%) are purified by filtering over a basic aluminium oxide plug and flushing with argon for 20 min prior to use. Methyl-2-bromopropionate (MBrP, Aldrich, 97%), *N,N,N',N',N'*-pentamethyl-diethylenetriamine (PMDETA, Aldrich, 99%) trifluoro acetic acid (TFA, Solvay Organics, 99%) zinc(II)acetate dihydrate (Merck, 99.5%),

cobalt(II)acetate tetrahydrate (Merck, 99%), sodium hydroxide (Fisher Chemicals, >97%), 1,4-dioxane (Applichem, 99%) dichloromethane (DCM, tech.) tetrahydrofuran (THF, VWR, 99.8%) and deuterated chloroform (CDCl₃, euriso-top, water < 0.01%, 99.8% D) are used without further purification. CuBr (Aldrich, 98%) is purified by suspension in concentrated acetic acid (Applichem, 100 %) for 12 h, filtering, washing with ethanol and diethylether, and vacuum drying at 75 °C for 72 h. Technical methanol, acetone and deionized water are used for the general work-up procedure.

Polymer synthesis

Model ionomers based on *n*BA and neutralized acrylic acid units of various molar fraction are synthesized in a three-step procedure by adapting literature protocols.^{32,29,28} In the first step, copolymers of *n*BA and *t*BA ($\chi_{tBA} = 0.5$ mol% – 10 mol%, see Table 1) are obtained by solvent-free atom-transfer radical polymerization (ATRP) with 0.128 mol% (based on the total comonomers) CuBr/PMDETA as catalyst, and 0.256 mol% MBrP as the initiator. The mixture is heated to 80 °C for 12 h. Subsequently, the reaction mixture is aerated and dissolved in acetone, filtered over neutral aluminum oxide to remove the catalyst, and precipitated in methanol/water (10:1 v/v) at -20 °C for 12h. Afterwards the copolymers are dried *in vacuo* (3 mbar) at 70 °C for 72 h (yield > 90 %). Subsequently, the *t*BA units are selectively hydrolyzed by dissolution in DCM at a concentration of 150 g·L⁻¹ and addition of 8 eq. of TFA relative to the amount of *t*BA units. The mixture is stirred for 48 h – 120 h and the reaction is monitored by ¹H-NMR followed by the same work up procedure as in the first step. The neutralization step is processed in 1,4-dioxane (10 mL·g⁻¹) by addition of the appropriate amount of either zinc(II)acetate dihydrate, cobalt(II)acetate tetrahydrate or sodium hydroxide as aqueous solution and stirring at 80 °C for 2 h. After removing the solvent under vacuum, the ionomer sample is homogenized by dissolving (10 mL·g⁻¹) in 1,4-dioxane/methanol (10:1 v/v), stirring at 80 °C for 2 h, removing the solvent under reduced pressure, and repeating the process twice. Afterwards, the materials are dried *in vacuo* (3 mbar) at 70 °C for 72 h. The polymers are encoded following the nomenclature: P*t*BA-X, PAA-X and PM-X; with *t*BA: poly(*tert*-butyl acrylate), AA: poly(acrylic acid), M: metal counter ion; P: poly(*n*-butyl acrylate) and X: mol% of *t*BA, AA or M. The balance is the *n*BA molar fraction.

Methods

¹H Nuclear magnetic resonance (¹H-NMR) spectroscopy of the pristine and hydrolyzed copolymers is performed using a Bruker DPX 300 (300.13 MHz) in CDCl₃ at room temperature. As an internal standard, the solvent signal is set to 7.26 ppm. Chemical shifts δ are assigned in ppm.

Size exclusion chromatography (SEC) is performed with THF as the eluent on a SEC system from hs GmbH, Germany, with the following components: pump (intelligent pump AI-12, Flow), degasser (Gastorr AG-32, Flow), autosampler (S5250, Sykam), RI-detector (RI2012 – A, Schambeck) and UV-detector (S3245 UV/Vis-detector, Sykam), and a column system (pre-column with 100 Å pore size and three columns of 10000 Å, 1000 Å and 100 Å, respectively) from MZ Analysentechnik; Germany with MZ-Gel SD plus as the stationary phase. Polystyrene standards (Polymer Laboratories) in the molar mass range of $M_w = 925$ g·mol⁻¹ - 1.98×10^6 g·mol⁻¹ are used for the calibration of the system.

Fourier-transformed infrared (FTIR) spectroscopy is recorded on a Shimadzu IR-Affinity-1 FTIR-spectrometer at room-temperature using an attenuated total internal reflectance (ATR) technique with 16 scans per measurement. The correlated bands are given in wave numbers ν [cm⁻¹].

Differential scanning calorimetry (DSC) measurements are performed in standard sealed aluminum containers using a heat-flux calorimeter DSC-1 (Mettler Toledo) with an empty aluminum container as reference between -80 °C and 180 °C at a heating rate of 10 K·min⁻¹ with an additional tempering step at 30 °C for 10 min. The data of the second heating run is used for analysis.

Frequency-dependent oscillatory rheology is carried out using an AR-G2 rheometer (TA Instruments) equipped with a plate-plate geometry with a diameter of 40 mm. All frequency sweeps are performed at 25 °C in a range of either 10⁻³ rad·s⁻¹ (or 10⁻¹ rad·s⁻¹, as indicated) to 628.3 rad·s⁻¹. The rubbery modulus G'_N characterizing the elastic regime is estimated at $\omega = \omega_{\text{cross}} + 10^3$ rad·s⁻¹ (ω_{cross} being the crossover angular frequency), or if this is beyond the measuring range, at the highest applicable frequency (628.3 rad·s⁻¹).

Tensile tests are performed on a zwicki Z2.5 (Zwick/Roell) with a AST IP53 KAF-IC 200 N load cell at 25 °C. The samples are prepared in a tailor-made pressing mold which is preheated to 100 °C in an oven before the stripes are pressed at 25 °C and 140 kg·cm⁻² for 45 min. All tests are performed on rectangular specimen cut to 25 mm x 3.3 mm x 2.5 mm. The elastic modulus $E = \lim_{\varepsilon \rightarrow 0} \left(\frac{\partial \sigma}{\partial \varepsilon} \right)$ is obtained by fitting the initial linear regime of the stress-strain curve. In preparatory cyclic tests, the specimen are subjected to a maximum elongation of $\varepsilon_{\text{max}} = 100$ % at various strain rates v_t , and relaxed to $\varepsilon = 0$ at the same strain rate. In standard tensile tests, at least three individual specimen are tested for each sample at a strain rate $v_t = 500$ mm·min⁻¹. For self-healing experiments, the stripes are center-cut perpendicular to the long axis along the short axis, and reunited to the original shape by bringing the freshly cut faces in close contact manually. Afterwards, the samples are simply placed in a conventional oven at a predetermined healing temperature and time period. Before using the healed stripes for tensile experiments, each sample is equilibrated at 25 °C for at least 2 hours.

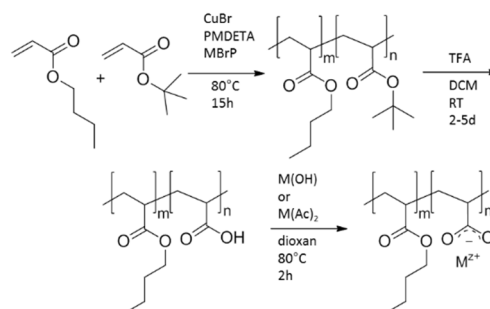
Small-angle X-ray scattering (SAXS) experiments are performed using a NANOSTAR camera (BrukerAXS, Germany) equipped with a μ S source, operated at 50 kV and 600 μ A. The wavelength is monochromatized to the Cu-K α line of 1.54 Å, with the sample-detector distance set to 1.06 m. Two-dimensional scattering patterns are collected on a multi-wired Vantec 2000 detector with a 2048 x 2048 resolution. Transmissions are obtained from absorbance measurements using a glassy carbon standard which is inserted in the optical path between sample and detector. All measurement data are corrected pixelwise for detector sensitivity, empty beam and dark current noise, and radially averaged. A flat diffuse scattering background is taken care of in the fitting procedures (see below). The intensities are absolutely calibrated in [cm⁻¹] to within 20 % - 30 % by means of a secondary standard that is calibrated before to water and Lupolene using the SAXS beamline, ID02 (ESRF, France) and SANS at KWS1 (Forschungszentrum Jülich, Germany) due to the difficulty of determining the exact thickness, i.e. the scattering volume of the samples.

Results and discussion

Inspired by recent promising findings concerning the intrinsic self-healing ability of ionomeric elastomers,^{33,34,10,23,24} the goal of the present work is the systematic investigation of the intercorrelation between ionomer composition, the nature of the counter ion, and the resulting bulk structure in connection with their mechanical and self-healing properties based on an accordingly designed model ionomer system. Our concept is based on a straight-forward synthetic approach that allows the tailored introduction of ionic groups along a fully amorphous main chain with a comparable molecular weight, and a narrow size distribution. This tactic ensures that the differences in the dynamic interactions between the macromolecules are dominated by the presence of ionic multiplets and clusters. A supramolecular network is formed that is crosslinked by the formation of ionic domains, and the required parameters of the system, i. e. the molecular architecture, the ionic fraction, and the counter-ion are controllable in a wide range. The supramolecular bond lifetime of the network nodes in such bulk materials is responsible for the materials response to external load, and serves as an important parameter to adjust the mechanical properties for optimization of the mechanical strength and self-healing ability.

Polymer synthesis and characterization

The parent copolymers based on *n*BA and *t*BA as the ionotropic component are prepared by copper-catalyzed ATRP in order to result in a linear structure, an adjustable and comparable molar mass and a narrow size distribution of the different materials that are compared. The employment of *n*BA as the main component, characterized by a glass transition temperature of the resulting matrix far below ambient, and *t*BA as the ionotropic comonomer has several advantages. As both monomers are of similar size and reactivity in the ATRP polymerization step, random copolymers are accessible with an adjustable composition. In addition, the *t*BA units are subsequently suitable for selective hydrolysis, resulting in carboxylic acid pendant groups that afterwards can be neutralized with different counter ions in a straight-forward way. The overall synthetic pathway is displayed in Scheme 2.



Scheme 2. Synthetic pathway to amorphous ionomers with a flexible backbone, adjustable ion fraction, and different counter ions ($M^{2+} = \text{Na}^+, \text{Zn}^{2+}, \text{Co}^{2+}$).

In preliminary rheology experiments on analogously prepared *n*BA homopolymers (not shown), it is verified that entanglements start to get important for the dynamic-

mechanical behavior only at a molar mass above $50,000 \text{ g}\cdot\text{mol}^{-1}$, in good accordance with findings in literature.^{35,36} Accordingly, for the present study we target a molar mass of the *n*BA/*t*BA parent copolymers in the range of $42,000 \text{ g}\cdot\text{mol}^{-1}$, in order to on the one hand ensure a maximum number of ionotropic groups per chain even for polymers with a low fraction of *t*BA, and on the other hand minimize the influence of entanglements on the resulting ionomer mechanical performance. The molar mass distribution of the copolymers is investigated by SEC, indicating that all samples fit into the target range ($42,000 \text{ g}\cdot\text{mol}^{-1} \pm 4,000 \text{ g}\cdot\text{mol}^{-1}$), and a successful control of the polymerization process is confirmed by a low polydispersity index (PDI ~ 1.1 , Table 1).

Table 1. Synthesis parameters and results on composition and molar mass analysis for *n*BA/*t*BA copolymers.

sample ^a	$\chi_{\text{BA},\text{syn}}$ [%]	$\chi_{\text{BA},\text{exp}}$ [%]	M_w [g·mol ⁻¹]	PDI	yield [%]
PtBA-0.3	0.5	0.3	35400	1.11	96.6
PtBA-0.4	0.5	0.4	44100	1.12	98.3
PtBA-2.0	2.0	2.0	41900	1.14	99.6
PtBA-2.6	3.0	2.6	40000	1.13	99.3
PtBA-4.2	4.0	4.2	39900	1.13	93.1
PtBA-5.2	5.0	5.2	38900	1.15	99.6
PtBA-6.2	6.0	6.2	46200	1.17	91.9
PtBA-8.6	8.0	8.6	45500	1.14	90.9
PtBA-9.2	9.0	9.2	43400	1.15	98.9
PtBA-9.9	10.0	9.9	40600	1.19	96.2

^a $\chi_{\text{BA},\text{syn}}$: *t*BA comonomer fraction during synthesis, $\chi_{\text{BA},\text{exp}}$: *t*BA comonomer fraction in the resulting copolymer according to ¹H-NMR, M_w : weight-average molar mass, PDI: polydispersity index (SEC).

The composition of the parent *n*BA/*t*BA copolymers is adjusted to a *t*BA molar fraction between 0.3 mol% and 10 mol%, and is counter-checked in the products by ¹H-NMR spectroscopy. A typical spectrum is shown in Figure 1. Based on the signals centered at 0.98 ppm (methyl protons in *n*BA) and 1.44 ppm (mainly caused by *n*BA β -methylene and *t*BA methyl protons),^{32,29} the *t*BA comonomer fraction of the polymers is found to be in good correspondence with the intended values (Table 1). A contribution of the main chain methylene protons to the signal at 1.44 ppm can be quantified from *n*BA homopolymers, and is appropriately taken into account for the calculation.

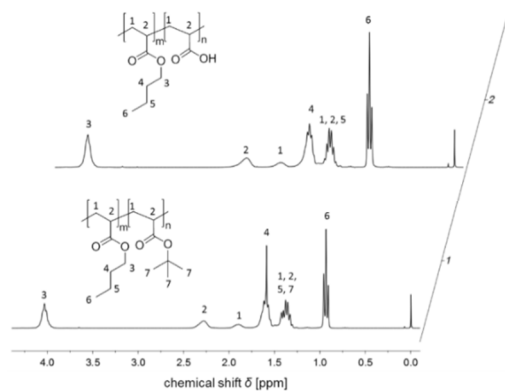


Figure 1. ¹H-NMR spectra of PtBA-2.6 (1) und PAA-2.6 (2) in CDCl₃.

The ester bonds of the *t*BA units in the parent copolymers are selectively hydrolyzed to pendant carboxylic acid groups by TFA in DCM. The progress of the reaction is followed by ¹H-NMR spectroscopy, and after a complete cleavage of the *t*BA ester bonds is indicated, the reaction is stopped. In the final products of this step, a hydrolyzation degree of $> 98 \%$ is accordingly verified using an analogous, ¹H NMR-based method.

After hydrolysis, the polymers are fully neutralized using either the appropriate amount of NaOH, Zn(II) acetate, or Co(II) acetate, respectively. The resulting ionomers are analyzed by FTIR spectroscopy. While the valence vibration band of the carbonyl function characteristic for the pendant *n*BA (or *t*BA) ester groups at about 1730 cm^{-1} is found in all spectra, including those of the parent polymers and of the hydrolyzed samples, the ionomer spectra additionally indicate the presence of coordinated metal carboxylate units in the area between $1585 \text{ cm}^{-1} - 1600 \text{ cm}^{-1}$. The exact wave number location and intensity of the latter depends on the nature of the counter ion and the overall ionic content.^{37,38} The intensity ratio of the two bands increases with increasing ion fraction (Figure 2 a, b).

The thermal characteristics of the parent copolymers and the corresponding hydrolyzed and neutralized polymers are investigated by DSC analysis, confirming the absence of a melt transition in all investigated samples (for a typical thermogram, see ESI). A weak influence of the copolymer composition on the matrix glass transition temperature T_g is observed for *n*BA/*t*BA parent copolymers, in accordance with the different glass transition temperatures of the bulk homopolymers of poly(*n*-butyl acrylate) ($T_g \sim -55 \text{ }^\circ\text{C}$)³⁹ and poly(*tert*-butyl acrylate) ($T_g \sim 70 \text{ }^\circ\text{C}$).⁴⁰ In comparison, the matrix T_g significantly depends on the composition for the hydrolyzed samples, manifesting the impact of pendant carboxylic acid groups and the related formation of hydrogen bonds (Figure 2c).³⁰ In the ionomers, the matrix T_g is similarly affected by the composition as in the hydrolyzed samples, yet is below $-25 \text{ }^\circ\text{C}$ in the whole composition range, indicating sufficient remaining segment mobility (for detailed results see ESI). The broadness of the glass transition considerably increases with increasing ionic content for all series. A second thermal transition is observed for ionomers with $\chi_{\text{ion}} > 2.5 \text{ mol}\%$ that is ascribed to the ionic transition T_{ion} . This transition is generally accepted to be the result of an ion-rich phase referred to as ionic multiplets, resulting in a region of restricted segment mobility. While T_{ion} is found to be around $50 \text{ }^\circ\text{C}$ for intermediate χ_{ion} , an increase up to $150 \text{ }^\circ\text{C}$ is observed for high ionic fractions, depending on the nature of the respective counter ion (Figure 2d). The latter can be explained by the accumulation of ionic multiplets into clusters. Based on the data available it can be assumed that the critical fraction for the cluster formation depends on the nature of the counter ion, and is observed at comparably lower ion fraction χ_{ion} for Na⁺-neutralized samples, as compared to Zn²⁺ and Co²⁺ neutralized samples.

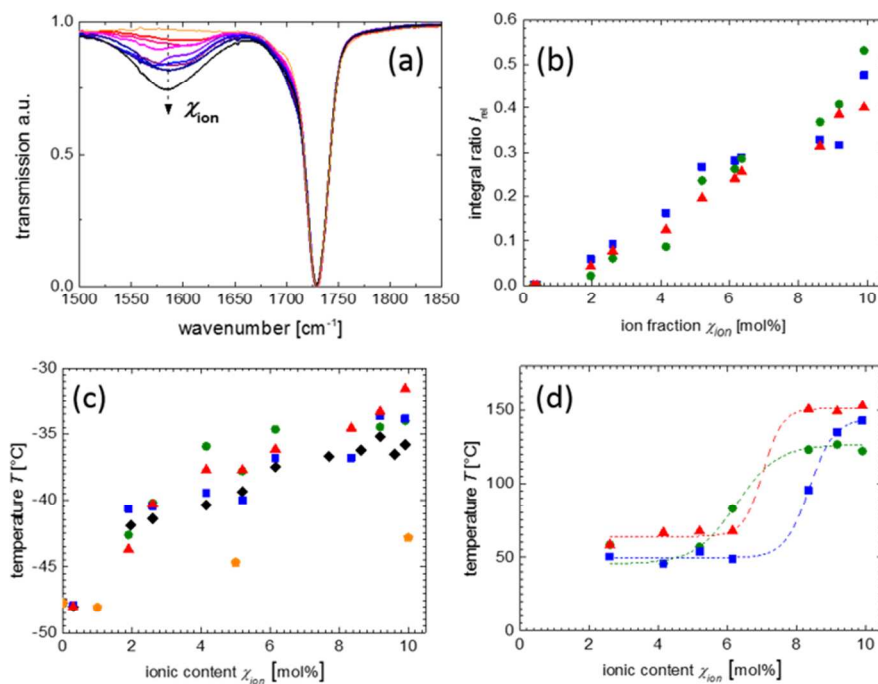


Figure 2. a) Normalized FTIR spectra of PCo-X with different ionic fraction χ_{ion} , b) integral ratio of the metal-carboxylate coordination band ($1580 \text{ cm}^{-1} - 1600 \text{ cm}^{-1}$) and ester band (1730 cm^{-1}) vs. ion fraction χ_{ion} c) matrix glass transition temperature T_g as obtained from DSC analysis of the parent (orange, pentagons), hydrolyzed (black, rhombs) and neutralized copolymers; d) ionic transition temperature T_{ion} of the ionomers vs. ionic fraction χ_{ion} , for PNa-X (green circles), PCo-X (blue squares) and PZn-X (red triangles.)

Structural characterization

In order to obtain information on the ionomer bulk morphology in dependence of the nature of the counter ion, SAXS experiments are carried out on selected samples. Figure 3c shows the SAXS scattering patterns of Na^+ , Zn^{2+} , and Co^{2+} -neutralized samples with a comparable ion fraction of ~ 4.5 mol%. The peak recognized around $q_{peak} \sim 0.1 \text{ \AA}^{-1}$ in all three samples is a clear signature of an interacting system of nanosized, ion-rich domains displaying a certain degree of order. The distance between the centers of mass D can be typically estimated from $D = 2\pi/q_{peak}$, however, the exact position of the maximum depends on the size and size distribution as well as on the degree of order of the clusters.

Until today there is no consensus as to which model of interaction for the ionic cluster domains is the most appropriate. The mutual arrangement of ionic aggregates in the matrix was treated in the literature partly by means of a hard-sphere interaction model, or of a version of para-crystalline order,

used earlier for the description of randomly distributed telechelic ionomers.^{41–47} Therefore in this manuscript we have opted to compare the classical hard sphere model with the mathematically more involved para-crystal model.

The presently covered q -range data on our samples should be ideally suited for a full determination of the structure information by SAXS, as the scattering intensity contains both the form factor of the ionic aggregates and the structure factor of the domain ensemble. We will always assume spherical morphologies as the most likely configuration of the ionic multiplets. So, we are independent from the determination of the aggregate size by a second method like e.g. TEM with all related uncertainties arising from the projection, possible artefacts from multilayer formation and shadowing. While morphological features in the expected size range can be clearly observed in TEM (Figure 3a, b), an exact sizing remains difficult due to the named side effects.

Inspection of the small angle X-ray scattering data (Figure 3c) reveals that the typical oscillations for well-defined

monodisperse (spherical) aggregates are widely missing, indicating that at least a moderate polydispersity is to be taken into account. Since the particle size distribution is neither known nor can be predicted a priori from the chemical building-up of the ionic clusters, we have assumed a normalized Gaussian distribution of the ionic cluster aggregate radius R_m with distribution σ .

Recognizing the weakness of determining both form and structure factor simultaneously from the rather smooth curves, we compare the approximation by different structure factor models in order to get hands on the reliability of our results.

The Percus-Yevick (PY) structure factor has been applied earlier to bulk ionomer phases, and we refer for the details to the literature^{45–47,44} and ESI. In the component decomposition of the fits into the two factors, $P(q)$ and $S(q)$, shown exemplary for PNa-4.2 in Fig. 4d, it is seen that oscillations from the structure factor S are counter-acted and annihilated by the form factor P , rendering it difficult-to-impossible to separate both contributions uniquely. For our purpose we here only report the radius of the equivalent hard sphere interaction radius R_d ($= D/2$) and the fitted volume fraction of the aggregates v_m (Table 2).

Based on the PY fitting parameters, the size $R_{m,PY}$ of the ion-rich aggregates decreases in the order of $Na > Zn > Co$, while the center distance R_d changes less significant. Moreover, for PNa-4.2 the results indicate that R_m is larger than R_d , being physically impossible in the PY model. This may be an artefact caused by a significant aggregate size distribution and/or

indicating that the assumption of a hard sphere interaction might be oversimplified.

Being aware of these limitations and in order to check the consistency, we compare the results with those obtained from a para-crystalline (PC) approach based on different lattice models (simple cubic (sc), body-centered cubic (bcc) and face-centered cubic (fcc), for details see ESI).

The results are summarized in Table 3 exemplarily for sample PNa-4.2. No significant difference is found between the calculations for bcc, fcc, and sc lattice models. The average size of the ionic clusters at the lattice points, $R_{m,PC}$ hardly differs between the different lattices, while the lattice constant a is affected more strongly, as expected from geometric considerations.

Table 2. Structural parameters for selected bulk ionomers based on different counter ions according to SAXS data using the hard sphere Percus-Yevick approach.

sample ^a	$R_{m,PY}$ [Å]	σ [Å]	$R_{d,PY}$ [Å]	v_m	N_m	V_m/N_m [nm ³]
PNa-4.2	45.2 ± 1.5	4.1 ± 0.3	34.4 ± 1.5	0.49 ± 0.03	~ 65	5.9
PZn-4.8	18.5 ± 0.6	4.9 ± 1.2	32.6 ± 0.6	0.18 ± 0.03	~ 32	0.76
PCo-4.2	7.4 ± 3.0	4.8 ± 3.0	25.0 ± 0.3	0.10 ± 0.03	~ 13	0.11

^a $R_{m,PY}$: mean aggregate radius (Gaussian), σ : sigma of the Gaussian distribution, $R_{d,PY}$: PY hard sphere interaction radius; v_m : fitted volume fraction of the aggregates, N_m : number of cations per aggregate (see text).

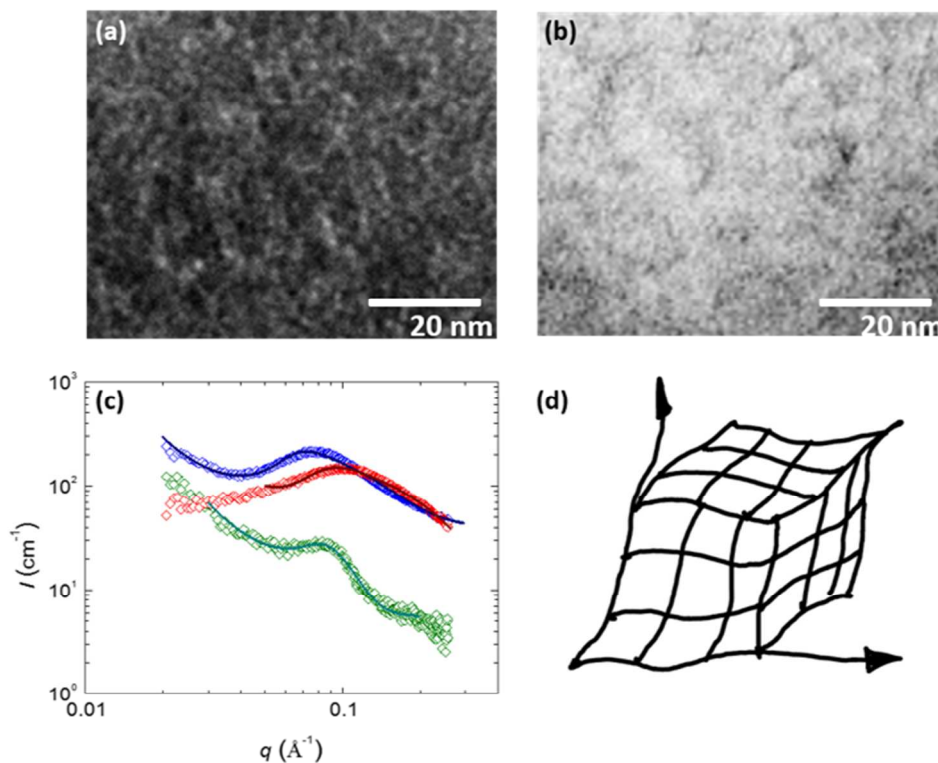


Figure 3. TEM images of PZn-5.2, drop casted on carbon grid, in a) bright-field b) and dark field imaging; c) SAXS data and corresponding fits for three ionomers with similar ionic fraction but different counter ions, PNa-4.2 (green), PZn-4.8 (red), and PCo-4.2 (blue), respectively; d) Scheme of a 3D paracrystalline morphology as applied in the PC model illustrating the irregularity of the unit cells.

Table 3. Structural parameters for PNa-4.2 according to SAXS data using the para-crystal theory.

lattice ^a	$R_{m,PC}$ [Å]	σ [Å]	a [Å]	$\Delta a/a$	$R_{d,PC}$ [Å]
bcc	42 ± 3	11 ± 1	86 ± 2	0.22 ± 0.01	37 ± 1
fcc	42 ± 3	11 ± 1	108 ± 2	0.24 ± 0.01	38 ± 1
sc	39 ± 2	11 ± 1	70 ± 1	0.25 ± 0.01	35 ± 1

^a $R_{m,PC}$: mean aggregate radius (Gaussian), σ : sigma of the Gaussian distribution; a : lattice constant; $\Delta a/a$: lattice constant distortion ratio; $R_{d,PC}$: equivalent hard sphere interaction radius; bcc: body-centered cubic, fcc: face-centered cubic, sc: simple cubic.

The values for the lattice constant distortion $\Delta a/a$ are of the order of 20 % - 25 % and indicative for a strong disorder on the length scale of the interactions. The fits can be barely distinguished from the hard sphere model fits and not shown.

The equally good agreement of the data with both the HS sphere model or para-crystalline structures is even more striking when the radius of the HS interaction, R_d , is compared with the size of the equivalent value R_{PC} in the paracrystal model. R_{PC} is calculated as the distance at which the particles are to touch each other from simple geometric considerations (see ESI for details). Within errors, the obtained values are in good correspondence with the much simpler (but rather unspecific) Percus-Yevick model, with $R_d \sim 34$ Å. A similar agreement is obtained for the other bivalent cationic clusters.

Based on the size and volume fraction of the multiplets as obtained from SAXS, the average number of cations per ionic aggregate N_m can be estimated sufficiently well based on the simple cubic lattice containing one spherical aggregate particle in the unit cell. We use the global carboxylate anion density in the sample ρ_{ion} (obtained from the ionomer composition χ_{ion} , the polymer specific density being close to 1.04 g·cm⁻³ for all samples, and the molar mass of the respective repeating units) to obtain the number of ions in a volume of $V_d = (2R_d)^3$. The latter yields directly N_m by assuming that all available cations and anions present in V_d are located in one ionic aggregate. As an additional information, the average volume of each cation in the ion-rich aggregates, V_m/N_m can be obtained as an estimate on how dense the ionic groups are packed. The results are summarized in Table 2.

The results indicate that simultaneously with the decrease in the size (R_m), the volume fraction v_m of the ionic-rich aggregates (with $v_m = (R_m/R_d)^3$) decreases in the order of PNa-X > PZn-X > PCo-X. The trend is accompanied with a decrease of the number of ionic groups in the aggregate N_m . In particular, in PNa-4.2, the fitted volume fraction of the ionic-rich (disperse) phase is nearly 50%, close to the closest packing in a body-centered cubic (bcc) arrangement. In the literature a transition from liquidlike ordering (i.e. Percus-Yevick-like) into more ordered states has been predicted to occur at 49%.⁴⁸ At the same time, the average volume per cation in the aggregates is

relatively high, indicating the presence of a significant fraction of polymer segments in the ion-rich phase.

For both the bivalent cations, the effective volume fraction of the aggregates is significantly lower. Consequently, as the ionomers exhibit a similar composition ($\chi_{ion} \sim 4.5$ %), the volume occupied by each cation is either smaller, or the ions show a closer packing in the ion-rich phase. Indeed, the value found for PCo-4.2 is close to the value reported for a single acid-ion pair.^{49,41}

While the results are in qualitative agreement and quantitative consensus with the trends reported previously,^{50,51,42,52,43} we are aware that the simple model we employ describes the material only very coarsely, and that a large variety of morphologies, including spherical aggregates, string-like structures and percolated networks⁵⁰ has previously been reported for ionomeric polymers with moderate to high ion fraction. However, the information on the general trend between the different cations will suffice for our purposes here, recognizing the crudeness of the approximation. We show below that the relative aggregate size (or rather, the equivalent sphere) and aggregate density are in correspondence with the quasi-static and dynamic mechanical behavior of the materials.

Summarizing the SAXS results for the ionomers, a good estimation of the aggregate size (i.e. the diameter of ion-rich domains) is possible by the application of different structural models, giving coinciding results and indicate a rather moderate size distribution and structural disorder. The domain size is largest for the Na-based ionomer, while the aggregation number is equally large, yet the packing density of the ions in the aggregates is lower than for the bivalent cations. For the purpose of this work that focuses on the self-healing properties of ionomers, the structural domain arrangement is considered to be of less importance in the first attempt, but may well be a valuable aspect in future studies.

Rheological properties

From oscillatory rheology, valuable information is available on the molecular dynamics and the time-dependent mechanical performance of the ionomer series in relation to their ion content and the nature of the counter-ion. In Figure 4a, typical results for the frequency-dependent storage and loss moduli (G' and G'') of the ionomers at 25 °C are presented for the series of Co²⁺-neutralized samples at different ion fractions. The spectra are characteristic for a more or less pronounced viscoelastic behavior of the samples, described by the crossover frequency ω_{cross} and the occurrence of a frequency-independent levelled-off modulus G'_N at frequencies beyond ω_{cross} , as expected for a dynamic network. While the former is a measure for the characteristic bond lifetime in dynamically crosslinked materials, the latter gives an estimate of the average segment length M_c between the network nodes, according to rubber

elasticity theory (see below). The spectra are principally similar for the Na⁺ and Zn²⁺ series, exhibiting a decrease of the crossover frequency (Fig 4c) and an increase of the modulus with increasing ion fraction. The observations are in accordance with the assumption that the ionic multiplets act as network nodes and/or nanofillers. While at low ionic fractions and frequencies, a Newtonian liquid-like behavior is observed, indicated by a constant η^* in the frequency domain (Figure 4b), ionomers with a moderate ionic fraction show a typical elastomeric behavior at high frequencies.⁵³

The effective average segment length M_c between two network nodes in the supramolecular networks can be calculated from G_N' assuming an affine network,^{54,55} for which G_N' is of the order of $k_B T$ per network strand, thus

$$M_c = \frac{\rho_p R T}{G_N'} \quad (1)$$

with R: gas constant (8.314 J·mol⁻¹·K⁻¹), T: temperature; ρ_p : polymer density (1.04 g·cm⁻³).

In Figure 4d, the experimental average segment length M_c is plotted against the ion fraction for all ionomers under investigation. Within the experimental limits, it is observed that M_c is similar for ionomers with an analogous ion fraction based on different counter ions. The results can be compared to the average length of a polymer segment between two ionic groups that is simply given by $M_\chi = M_{nBA}/\chi_{ion}$, shown as the dotted line in Figure 4d. Deviation from this expectation is found for ionomers with an ionic fraction of as high as 10 %, probably caused by percolation effects or a change in morphology.

Interestingly, independent of the nature of the counter ion, the segment length M_c as extracted from G_N' is similar to M_χ , demonstrating that the ionic groups along the main chain serve as effective branching points or crosslinks. Thus, the elastic behavior observed in the high frequency regime is dominated by the ionic interaction between individual chains, and seems to be less influenced by the aggregation number. A purely affine rubber elastic behavior is expected if the crosslink functionality i.e. the number of chains emanating from the domains tend to infinity. At the same time, no significant filler effect on the dynamic rheometric properties associated with the presence of the ionic aggregates is observed. If we take into account that the size of the elastic mesh between potential sticker positions depends on the ionic fraction, this roughly corresponds to an affine M_c value of ~2500 gmol⁻¹ for an ionomer with an ionic fraction of 5 %. This is comparable to the entanglement molecular mass of a simple polyethylene of which the plateau modulus G_e is about 1 MPa, thus in accordance with the data given in table S2. On the other hand, the multiplet diameter as obtained by SAXS (20 Å - 100 Å) is comparable with the estimated radius of gyration (60 Å). Under the given conditions, we can thus consider the multiplets as nanofillers, and in a first approximation we can estimate that the increase in the modulus depends on the relative volume fraction as $G_n =$

$G_{n,\phi=0} \cdot (1 + 2/5 \phi)$ for hard particulate fillers. The real effect, however, is much weaker due to the increasingly soft nature of the ionic multiplets: At high volume fractions and increasing size of the multiplets, it is from compositional considerations very likely that the clusters are protruded by polymeric backbones which render the domains plastically deformable.

While the segment length M_c as extracted from G_N' for a given composition seems not to depend strongly on the type of counter ion, the dependence of the crossover frequency ω_{cross} on the ionic fraction differs for the three ionomer series. As shown in Figure 4c, the impact of χ_{ion} on ω_{cross} is strongest for the Co²⁺ neutralized series, and is less pronounced in the Zn²⁺ and Na⁺ neutralized series. In particular, in the Co²⁺-based series, the crossover frequency ω_{cross} quickly approaches values below 10² s⁻¹, and thus gives rise to a predominantly elastomeric mechanical response under standard load conditions in the application case, as verified in tensile experiments (see below). For ionomers with high ion fraction, ω_{cross} is beyond the lower measuring range.

The crossover frequency quantifies the terminal relaxation time (flow onset) that is a good estimate of the lifetime of an ionic crosslink, or rather the average residence time of an ionic group within an individual cluster, $\tau_d = 2\pi/\omega_{cross}$. While in the context of the present study, we focus on the room temperature rheological behavior that is related to the materials' mechanical performance under working conditions, in a related paper⁵⁶ we extend the investigation to elevated temperatures, demonstrating a direct correlation of ω_{cross} and the plateau modulus in these model ionic elastomers, and argue that both values are ideally adjusted to result in good self-healing properties.

In addition, the complex shear viscosity η^* of Na⁺, Zn²⁺ and Co²⁺ neutralized samples with an ionic fraction of $\chi_{ion} = 4.2$ mol% is compared in Figure 4b. In accordance with the relative course ω_{cross} and G'' of in the three series, PNa-4.2 and PZn-4.2 show a liquidlike behavior at low frequencies, indicated by the Newtonian plateau in η^* , while the response of PCo-4.2 is typical for an elastomer in the investigated frequency range.

The low-frequency behavior is interpreted as a contribution of the long-time interaction between an individual chain with its direct neighbours via the ionic multiplets. The number of active sticker groups per chain averaged over time is proportional to the number of potential stickers (ionic groups) per chain, and the probability p of an individual ionic group to be part of a multiplet. This probability is determined by the average life times of the bound and the free state, respectively, and therefore is affected by the nature of the counter ion. According to the preset data, the complex viscosity and low frequency of the ionomers increases in the order $\eta_{PNa}^* < \eta_{PZn}^* < \eta_{PCo}^*$, indicating an increasing p in the same direction. This is accordance with other observations from rheology, such as longer relaxation times.

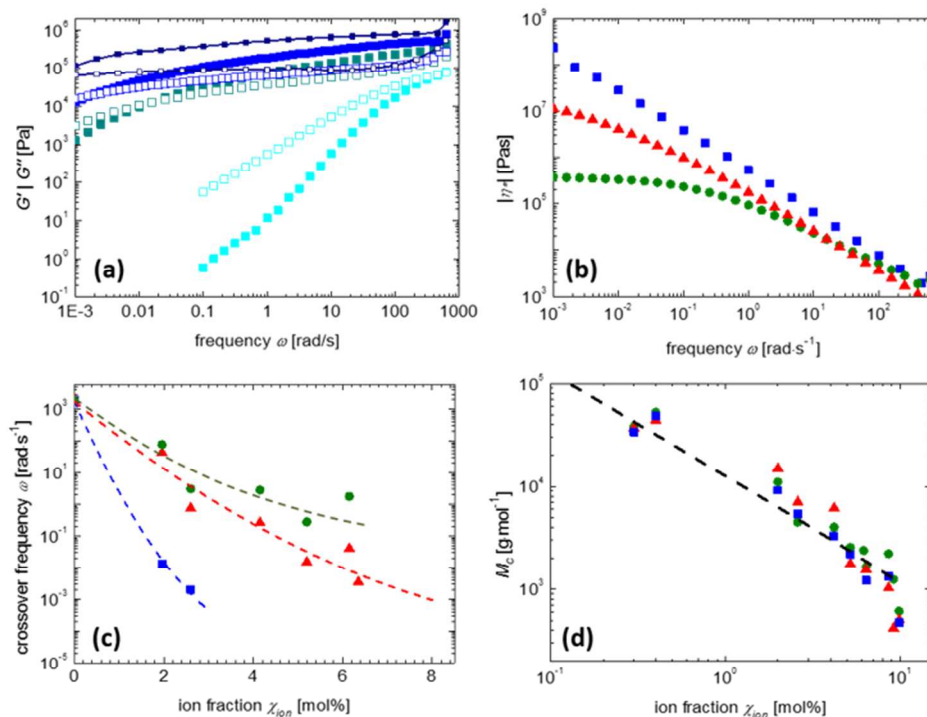


Figure 4. a) Frequency-dependent shear storage modulus G' and shear loss modulus G'' of PCo-X with X: 0.3 (cyan), 2.0 (blue) and 2.6 (marine), 5.2 (dark blue); b) complex shear viscosity η^* of PM-4.2 vs. frequency ω ; c) crossover frequency ω_{cross} vs. ion fraction χ_{ion} of PM-X; d) average effective segment length M_c in PM-X vs. ion fraction χ_{ion} , based on G'_N , with M: Na (green circles), Co (blue squares) and Zn (red triangles).

The high-frequency behavior is similar in the three series, in accordance with the observation, that the plateau modulus of polymers with the same ion fraction, but different counter ion is similar.

The observation that the segment length M_c derived from the modulus level is a universal function of the ion fraction χ_{ion} , and does not reflect the qualitative differences among the samples with different counter ions seen by SAXS, is ultimately in accordance with the hypothesis that the ionic groups serve as the effective crosslinking moieties. At the same time, the kinetics in the dynamic crosslinks, represented by the residence time τ_d , and its dependence on the ion fraction, depends on the nature of the counter ion, and τ_d increases in the order PNa-X < PZn-X < PCo-X. This trend might be related to the packing density of the ionic groups within the ion-rich domains as estimated by SAXS. The latter can be considered to be characteristic for the extent of phase separation.

Tensile properties

The mechanical properties under uniaxial deformation and the self-healing performance are investigated in tensile experiments at 25 °C for ionomers with an ionic fraction χ_{ion} of 5.2 mol% and higher. At a lower fraction of ions, the viscous component of the materials mechanical response becomes more important, giving rise to extended creep and related effects, and the mechanical properties under quasi-static load conditions become non-revocable. For $\chi_{\text{ion}} > 5.2$ mol%, however, the materials show tensile curves that are typical for thermoplastic elastomers, characterized by a moderate elastic modulus E , high extensibility, and nearly complete recovery of the initial shape after unloading. In preliminary experiments, we certified the reversibility of the deformation and independence of the elastic modulus of the strain rate for rates of 100 mm·s⁻¹ and higher (more details can be found in the ESI).

Typical tensile graphs for a series of PZn-X drawn to break at 500 mm·s⁻¹ are shown in Figure 5a. Although no systematic optimization of the sample preparation procedure is applied, and although chemical crosslinks are absent, the ionomers with a moderate ion fraction show a high extensibility up to $\epsilon_R = 350$

%, and an excellent tensile strength σ_{\max} up to 5 MPa. With increasing ion fraction, an increase of σ_{\max} and the elastic modulus E , and a decrease of ε_{R} is found. While the elastic modulus E is similar for Na^+ -, Zn^{2+} , and Co^{2+} -neutralized samples with 5.2 mol%, the increase of the modulus with ion fraction is only weakly pronounced for the PNa-X series, while showing a similar trend for the PZn-X and PCo-X series (see Figure 5b and ESI). For several samples, we find a good indication of the theoretically expected relation $E = 3G$.

In accordance with rheology, the PNa-X series is thus the softest materials, where the ionic aggregates seem to have a comparable small impact in terms of mechanical strengthening. This is confirmed by the trends in complex viscosity η^* and cross-over frequency, as obtained by rheology. In view of the SAXS results (see above), this is in accordance with a comparably weak phase separation in the respective ionomers, and/or a loose packing of the ion groups in the aggregate, in connection with a relatively high chain mobility as indicated by ω_{cross} (or residence time τ_{d}). It should be pointed out that the

carboxylate anion, characterized by a single, delocalized negative charge, is a soft anion with a high affinity to soft cations like d-transition metal cations according to Pearson's HSAB concept. In contrast, Na^+ is a single-charged, comparable hard cation, with a significantly different coordination behavior for carboxylates. The results thus point to a different aggregation behavior in the PNa-X series as compared to the other two series based on soft, bivalent d-metals. This aspect is further analyzed by FT-IR rheology in a related paper.⁵⁶

Nevertheless, the respective trends observed within one ionomer series, and the qualitative comparison among the different series indicate a straight-forward interrelation between the ionomer composition, morphology, and mechanical performance. By knowledge of these relationships, it becomes possible to tailor the ionic interactions in an ionomeric material towards the specific needs in a particular application.

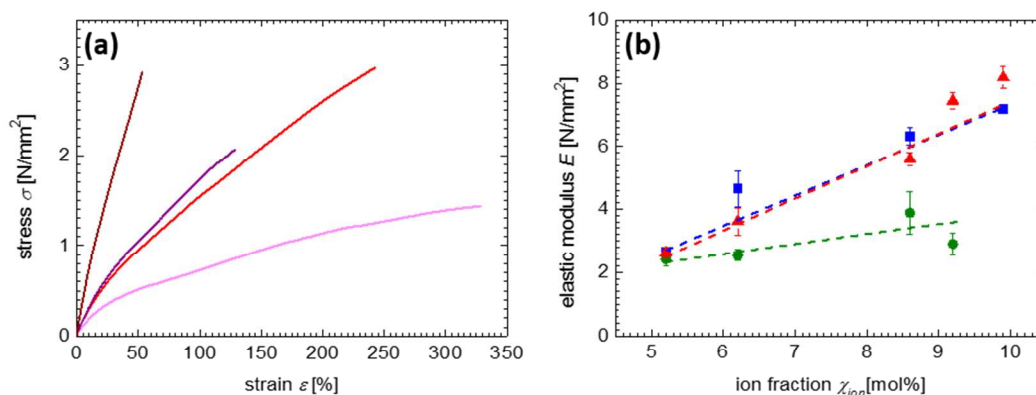


Figure 5. a) Stress-strain curves of PZn-X with X: 5.2 (magenta), 6.2 (red), 6.4 (purple) and 9.2 (brown); b) elastic modulus E of of PM-X vs. ion fraction χ_{ion} with M: Na (green circles), Co (blue squares) and Zn (red triangles).

Self-healing efficiency

While it is traditionally accepted that the interchain interactions in an ideal elastomer are permanent and instantaneously, the ongoing investigation of self-healing materials reveals that an ideal self-healing elastomer has both: high mechanical integrity under load conditions, while on long timescales (or at enhanced temperatures), the chain and bond dynamics allow for an intrinsic repair of microcracks occurred during operation and aging. For the present system it can thus be assumed that an optimization of the self-healing properties in acrylate-based ionomers is based on the proper choice of counter ion with a high affinity for carboxylates. Furthermore, the ion fraction needs to exceed 5 mol% in order to allow sufficient mechanical stability under load conditions. As known from dynamic rheology, this is accompanied with a high residence time ($\tau_{\text{d}} > 100$ s). In addition, the thermal properties, in particular, the

ionic transition temperature T_{ion} should be in a range that allows for a thermal acceleration of the self-healing process. Although the materials should theoretically be accessible also to an autonomous self-healing process, the self-arrangement after damage can be accelerated by enhancing the temperature, while it is verified that the bulk sample is not subjected to macroscopic flow, but is shape-persistent during the healing process.

Based on these considerations, we investigate the self-healing efficiency of the ionomeric elastomers with $\chi_{\text{ion}} > 5$ mol% in cut-and-heal tensile tests in more detail. For the same materials, self-healing experiments based on scratch experiments are presented in Ref.⁵⁷. In the present experiments, ionomer specimen obtained in a tailor-made polymer press and cut into rectangular stripes, are carefully center-cut in half along the short axis, thus perpendicular to the later strain direction. Afterwards, the pieces are reunited by bringing the freshly cut

faces in close contact manually, taking advantage of the faces still being self-adhesive when freshly cut (in contrast to aged cut faces). Afterwards, the samples are simply placed in a conventional oven at a given temperature for a predetermined time. The mechanical performance of the healed samples is investigated by tensile tests at room temperature, and compared to that of the uncut, pristine material. Accordingly, the healing efficiency μ is determined based both on the elongation at break ε_R

$$\mu_\varepsilon = \frac{\varepsilon_R}{\varepsilon_{R,0}} \quad (2)$$

and on the tensile strength σ_{\max} .

$$\mu_\sigma = \frac{\sigma_{\max}}{\sigma_{\max,0}} \quad (3)$$

Ionomers with an ionic fraction of about 5 mol% have previously shown high healing efficiencies at short healing times.⁵⁷ In initial experiments it was verified that in order to result in good and reproducible healing properties, a contact time at 80 °C for 30 min is sufficient for PM-X (M: Na, Zn, Co) series, see Fig. 6 e and f. Accordingly, these conditions are a good standard to investigate the influence of the ionomer composition. While ionomers of the PM-X (M: Na, Zn, Co)

series with different ion fractions are compared for their healing properties based on these standard conditions, the healing temperature and time is additionally investigated for the ionomer with the best healing performance, PM-5.2.

The results are presented in Figure 6. While all materials under investigation show a significant healing behavior, an almost complete recovery of the mechanical performance is observed for PM-5.2 under standard conditions (Figure 6b), with healing efficiencies μ_ε and μ_σ beyond 90 %. Materials with a higher ion fraction indicated lower healing efficiencies under the same healing conditions, probably attributed to slower molecular mobility as indicated by the high residence time τ_d (low wcross, Fig. 4c), and high ionic transition temperature T_i (Figure 2d), thus in accordance with the internal dynamics being the dominating parameters.

More information obtained by thermorheology is presented in our other paper.⁵⁶

As shown in Figure 6 c and d, all samples with an ionic fraction of 5.2 mol% show excellent healing efficiency μ_σ after 30 min at 80 °C. At 60 °C, the results for the Co- and Zn-based sample are similar good, while at 40 °C, the healing process is obviously still incomplete after 30 min, probably attributed to the fact that this is below T_i . For the Na-based sample, the healing efficiencies at 40 °C and 60 °C are considerably lower than for the bivalent cations.

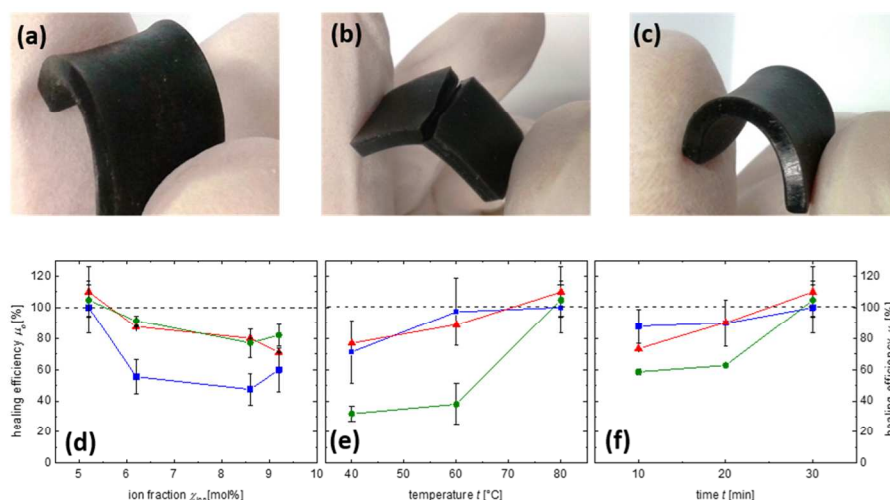


Figure 6. a-c) PCo-5.2 specimen used in cut-and-heal experiments: a) reference, b) cut edges in contact for 24 h at 25 °C, c) for 30 min at 80 °C, d-f) self-healing efficiency based on the tensile strength, μ_σ , of various ionomers PM-X with M = Na (green circles), Co (blue squares) and Zn (red triangles) in dependence of the d) ion fraction x_{ion} (30 min at 80 °C), e) temperature T ($t = 30$ min), and f) time t ($T = 80$ °C) for PM-5.2.

The time dependence of the healing process for the three samples shows a similar trend. While the Co- and Zn-based samples are already fully healed after 20 min, the Na-based sample has the slowest healing progress. In our other paper,⁵⁷ we present the time dependence of the thermal scratch healing process for PCo-6 and PZn-6 ionomers, and generally found a

similar behavior. While the healing efficiency based on scratch closure was found to be around 50 % after 30 min at 50 °C, we found a somewhat faster recovery of the tensile strength here (~70 % at 40 °C). At 100 °C, scratches were fully healed after 30 min, in agreement with our observation that PM-5.2 ionomers are fully healed after the same time already at 80 °C. The processes are thus active in similar temperature ranges and on

similar time scales, and are in qualitative accordance with the cited values for the activation energy E_a . The latter follows the trend of E_a (PCo) > E_a (PZn) > E_a (PNa), and increases with ionic fraction (1 – 10 %) between 40 and 150 kJ·mol⁻¹.⁵⁷ In accordance with these considerations, the observed self-healing profiles correspond to the general trends expected from (thermo)rheology, and all findings indicate that ionomers of the PM-5.2 series show a good compromise good mechanical performance and fast self-healing at moderate conditions.

These principal investigations on the self-healing properties of ionomeric elastomers can be translated into a general guideline for the design of similar materials and the tailored adjustment of their mechanical properties with optimized self-healing efficiency. While the behavior under dynamic load, thus in the elastic regime, is mainly determined by the fraction of ions in the materials, the time scale of the viscous-to-elastic transition (given by ω_{cross}) is influenced by the nature of the counter ion. Further parameters that need to be taken into account are the polarity of the matrix that is of importance for the phase separation and aggregate formation, and finally the thermorheological properties in the case of a thermally activated healing process. This latter aspect is addressed in more detail elsewhere.⁵⁶

Conclusions

In order to investigate the relationship between composition, morphology, and thermal and mechanical performance in self-healing ionomeric elastomers, acrylate-based amorphous ionomers with a systematic property variation are presented and analyzed by a combination of methods, including DSC, SAXS, dynamic rheology, and tensile tests. Three series of ionomers with pendant carboxylate groups arising from full neutralization with either Na⁺, Zn²⁺ or Co²⁺ are compared over a wide range of compositions. Our results indicate the correlation between the ion fraction and the temperature of the ionic transition to display a critical clustering concentration of ionic multiplets depending on the nature of the counter ion. The aggregation number and size of the ionic multiplets as investigated by SAXS and reveal an aggregate size between 7 Å and 45 Å.

In dynamic-mechanical experiments by oscillating rheology at ambient temperature, the direct impact of the ion fraction on the network modulus G'_N (reflecting the effective crosslinking density) is confirmed, while the characteristic bond lifetime of the network nodes varies with the counter ion employed. The general trend is similarly manifested in the tensile properties of ionomers with an ion fraction of 5 % and higher, showing an overall performance characteristic for thermoplastic elastomers. By cut-and-heal experiments, the self-healing efficiency based on the tensile strength and elongation-at-break is investigated and optimized by comparing the respective tensile properties to the pristine materials. In Co²⁺-based ionomers with moderate ion fraction, a nearly total recovery of the mechanical properties is found after short healing times at moderate temperature.

The findings are of importance for the understanding of the underlying principles for self-healing and effective crosslinking in ionomeric elastomers, and can be employed to similar adaptive systems based on dynamic bonds.

Acknowledgements

This work is supported by the DFG priority program SPP 1568 “Design and Generic Principles of Self-healing Materials”.

Notes and references

^a Universität zu Köln, Chemistry Department, Luxemburger Str. 116, D-50939 Cologne, Germany, E-Mail: annette.schmidt@uni-koeln.de

^b Forschungszentrum Jülich, Jülich Centre for Neutron Science-1 and Institute for Complex Systems-1, Wilhelm-Johnen-Straße, D-52428 Jülich, Germany

Electronic Supplementary Information (ESI) available: Details on the thermal and mechanical characterization and on the SAXS model. See DOI: 10.1039/b000000x/

1. X. Yan, D. Xu, X. Chi, J. Chen, S. Dong, X. Ding, Y. Yu, and F. Huang, *Adv. Mater.*, 2012, **24**, 362–9.
2. E. B. Murphy and F. Wudl, *Prog. Polym. Sci.*, 2010, **35**, 223–251.
3. P. Cordier, F. Tournilhac, C. Soulié-Ziakovic, and L. Leibler, *Nature*, 2008, **451**, 977–80.
4. R. J. Varley and S. van der Zwaag, *Polym. Int.*, 2010, **59**, 1031–1038.
5. J. Zhou, A. M. Schmidt, and H. Ritter, *Macromolecules*, 2010, **43**, 939–942.
6. P. Brown, A. Bushmelev, C. P. Butts, J. Cheng, J. Eastoe, I. Grillo, R. K. Heenan, and A. M. Schmidt, *Angew. Chem. Int. Ed. Engl.*, 2012, **51**, 2414–6.
7. T. Speck, M. von Tapavicza, A. Nellesen, A. M. Schmidt, and R. Müllhaupt, in *Materials design inspired by Nature: Function through inner Architecture*, ed. R. W. P. Fratzl, J. W. C. Dunlop, RSC Publishing, 2013.
8. M. D. Hager, P. Greil, C. Leyens, S. van der Zwaag, and U. S. Schubert, *Adv. Mater.*, 2010, **22**, 5424–30.
9. N. Holten-Andersen, M. J. Harrington, H. Birkedal, B. P. Lee, P. B. Messersmith, K. Y. C. Lee, and J. H. Waite, *Proc. Natl. Acad. Sci. U. S. A.*, 2011, **108**, 2651–5.
10. D. Döhler, P. Zare, and W. H. Binder, *Polym. Chem.*, 2014, **5**, 992.
11. J.-M. Lehn, *Prog. Polym. Sci.*, 2005, **30**, 814–831.
12. A. R. Bras, W. Pyckhout-Hintzen, A. Wischniewski, and D. Richter, in *Self-Healing Polymers - from Principles to Applications*, ed. W. H. Binder, Wiley-VCH, 2014.

13. A. Eisenberg, B. Hird, and R. B. Moore, *Macromolecules*, 1990, **23**, 4098–4107.
14. A. Eisenberg and M. Rinaudo, *Polym. Bull.*, 1990, **24**, 671.
15. L. Holliday, *Ionic Polymers*, Applied Science Publishers, 1975.
16. W. J. MacKnight and T. R. Earnest, *J. Polym. Sci. Macromol. Rev.*, 1981, **16**, 41–122.
17. Eisenberg A. and J.-S. Kim, *Introduction to Ionomers*, Wiley, New York, 1998.
18. M. A. Rhaman, M. Penco, G. Spagnoli, A. M. Grande, and L. Di Landro, *Macromol. Mater. Eng.*, 2011, **296**, 1119–1127.
19. S. J. Kalista and T. C. Ward, *J. R. Soc. Interface*, 2007, **4**, 405–11.
20. R. J. Varley, S. Shen, and S. van der Zwaag, *Polymer (Guildf.)*, 2010, **51**, 679–686.
21. M. A. Aboudzadeh, M. E. Muñoz, A. Santamaría, R. Marcilla, and D. Mecerreyes, *Macromol. Rapid Commun.*, 2012, **33**, 314–8.
22. S. J. Garcia, *Eur. Polym. J.*, 2014, **53**, 118–125.
23. S. Tungchaiwattana, M. S. Musa, J. Yan, P. a Lovell, P. Shaw, and B. R. Saunders, *Soft Matter*, 2014, **10**, 4725–34.
24. M. A. Malmierca, A. Gonzales-Jimenez, I. Mora-Barrantes, P. Posadas, A. Rodriguez, L. Ibarra, A. Nogales, K. Saalwächter, and J. L. Valentin, *Macromolecules*, 2014, **47**, 5655–5667.
25. N. Hohlbein, M. von Tapavicza, A. Nellesen, and A. M. Schmidt, in *Self-healing polymers - from principles to applications*, ed. W. H. Binder, Wiley-VCH, 2013.
26. R. J. Varley, in *Springer Series in Materials Science, Vol. 100: Self Healing Materials*, 2007, pp. 95–114.
27. A. Schüssele, University of Freiburg, 2012.
28. P. Vanhoorne and R. a. Register, *Macromolecules*, 1996, **29**, 598–604.
29. O. Colombani, M. Ruppel, F. Schubert, H. Zettl, D. V. Pergushov, and A. H. E. Müller, *Macromolecules*, 2007, **40**, 4338–4350.
30. Q. Ma and K. L. Wooley, *J. Polym. Sci. Part A Polym. Chem.*, 2000, **38**, 4805–4820.
31. W. a. Braunecker and K. Matyjaszewski, *Prog. Polym. Sci.*, 2007, **32**, 93–146.
32. Q. Ma and K. L. Wooley, *J. Polym. Sci. Part A Polym. Chem.*, 2000, **38**, 4805–4820.
33. A. M. Grande, L. Castelnovo, L. Di Landro, C. Giacomuzzo, A. Francesconi, and M. A. Rahman, *J. Appl. Polym. Sci.*, 2013, **130**, 1949–1958.
34. M. A. Rahman, G. Spagnoli, A. M. Grande, and L. Di Landro, *Macromol. Mater. Eng.*, 2013, **298**, 1350–1364.
35. A. Zosel and G. Ley, *Macromolecules*, 1993, **26**, 2222–2227.
36. C. Former, J. Castro, C. M. Fellows, R. I. Tanner, and R. G. Gilbert, *J. Polym. Sci. Part A Polym. Chem.*, 2002, **40**, 3335–3349.
37. K. Han and H. L. Williams, *J. Appl. Phys.*, 1991, **42**, 1845–1859.
38. E. Hirasawa, H. Yamamoto, K. Tadano, and S. Yano, *J. Appl. Polym. Sci.*, 1991, **42**, 351–362.
39. U. Gaur, S. -f. Lau, B. B. Wunderlich, and B. Wunderlich, *J. Phys. Chem. Ref. Data*, 1982, **11**, 1065–1089.
40. A. R. Monahan, *J. Polym. Sci. Part A-1*, 1966, **4**, 2381–2390.
41. N. Zhou, C. Chan, and K. Winey, *Macromolecules*, 2008, **41**, 6134–6140.
42. K. I. Winey, J. H. Laurer, and B. P. Kirkmeyer, *Macromolecules*, 2000, **33**, 507–513.
43. B. P. Kirkmeyer, R. a. Weiss, and K. I. Winey, *J. Polym. Sci. Part B Polym. Phys.*, 2001, **39**, 477–483.
44. F. J. Stadler, W. Pyckhout-Hintzen, J.-M. Schumers, C.-A. Fustin, J.-F. Gohy, and C. Bailly, *Macromolecules*, 2009, **42**, 6181–6192.
45. D. J. Kinning and E. L. Thomas, *Macromolecules*, 1984, **17**, 1712–1718.
46. D. J. Yarusso and S. L. Cooper, *Macromolecules*, 1983, **16**, 1871–1880.
47. J.-P. Hansen and I. R. McDonald, *Theory of Simple Liquids*, Academic Press, London, 2nd edn., 1986.
48. W. G. Hoover, *J. Chem. Phys.*, 1968, **49**, 3609.
49. N. M. Benetatos, C. D. Chan, and K. I. Winey, 2007, 1081–1088.
50. D. S. Bolintineanu, M. J. Stevens, and A. L. Frischknecht, *ACS Macro Lett.*, 2013, **2**, 206–210.
51. N. C. Zhou, C. D. Chan, K. I. Winey, and V. Pennsylv, 2008, 6134–6140.
52. B. P. Kirkmeyer, A. Taubert, J.-S. Kim, and K. I. Winey, *Macromolecules*, 2002, **35**, 2648–2653.
53. R. K. Bose, N. Hohlbein, S. J. Garcia, A. M. Schmidt, and S. van der Zwaag, *Phys. Chem. Chem. Phys.*, 2015, **17**, 1697–1704.
54. M. Rubinstein, *Polymer Physics*, Oxford University Press, Oxford, 2003.
55. L. R. G. Treloar, *The Physics of Rubber Elasticity*, Clarendon, Oxford, 3rd edn., 2005.

ARTICLE

Journal Name

56. R. K. Bose, N. Hohlbein, S. J. Garcia, A. M. Schmidt, and S. van der Zwaag, *Phys. Chem. Chem. Phys.*, 2014.
57. R. K. Bose, N. Hohlbein, S. J. Garcia, A. M. Schmidt, and S. van der Zwaag, *Phys. Chem. Chem. Phys.*, **accepted**.

For Table of Contents use only

Self-healing Dynamic Bond-based Rubbers: Understanding the Mechanisms in Ionomeric Elastomer Model Systems

N. Hohlbein¹, A. Shaaban¹, A. R. Bras², W. Pyckhout-Hintzen², A. M. Schmidt^{1*}

¹ *Universität zu Köln, Chemistry Department, Luxemburger Str. 116, D-50939 Cologne, Germany*

² *Forschungszentrum Jülich, Jülich Centre for Neutron Science-1 and Institute for Complex Systems-1, Wilhelm-Johnen-Straße, D-52428 Jülich, Germany*

*E-Mail: annette.schmidt@uni-koeln.de

